Voltage controlled iontronic switches: a computational method to predict electrowetting in hydrophobically gated nanopores

Gonçalo Paulo, Alberto Gubbiotti, Giovanni Di Muccio & Alberto Giacomello

Published online: 10 Jan 2024.

Submit your article to this journal ↗

Article views: 332

View related articles ↗

View Crossmark data ↗

Taylor & Francis
Taylor & Francis Group

Voltage controlled iontronic switches: a computational method to predict electrowetting in hydrophobically gated nanopores

Gonçalo Paulo, Alberto Gubbiotti, Giovanni Di Muccio and Alberto Giacomello

Dipartimento di Ingegneria Meccanica e Aerospaziale, Sapienza Università di Roma, Rome, Italy

ABSTRACT

Reliable and controllable switches are crucial in nanofluidics and iontronics. Ion channels found in nature serve as a rich source of inspiration due to their intricate mechanisms modulated by stimuli like pressure, temperature, chemical species, and voltage. The artificial replication of the properties of these channels is challenging due to their complex chemistry, limited stability range, and intricate moving parts, allosterically modulated. Nonetheless, we can harness some of the gating mechanisms of ion channels for nanofluidic and iontronic purposes. This theoretical and computational study explores the use of electrowetting in simple hydrophobic nanopores to control their conductance using an external applied voltage. We employ restrained molecular dynamics to calculate the free energy required for wetting a model nanopore under different voltages. Utilizing a simple theory, we generate free energy profiles across a wide voltage range. We also computed transition rates between conductive and non-conductive states, showing their voltage dependence and how this behavior can impair memory to the system, resembling the memristor behavior voltage-gated channels in the brain. The proposed framework provides a promising avenue for designing and controlling hydrophobic nanopores via electrowetting, enabling potential applications in neuromorphic iontronics.
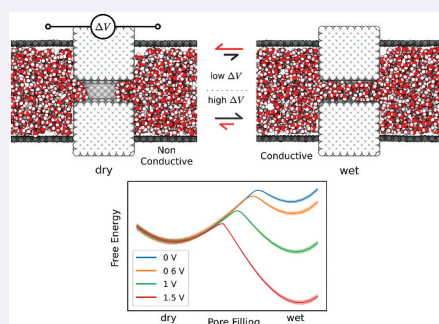
CONTACT Alberto Giacomello ✉ alberto.giacomello@uniroma1.it 🏛 Dipartimento di Ingegneria Meccanica e Aerospaziale, Sapienza Università di Roma, via Eudossiana, 18, Rome 00184, Italy

Introduction

Nature has long been a wellspring of inspiration for scientific innovation, offering intricate designs and dynamic processes that have fuelled advances across various domains [1,2]. It can demonstrate some of the best examples of both iontronics [3] – exemplified by the propagation of the action potential [4] – and nanofluidics, by presenting us with the complex machinery that are ion channels and many other biological pores, capable of a highly specialized modulation of the signaling and transport of ions, water and biological molecules across the cell membranes [5,6].

The complex transport properties of such membrane proteins are modulated by their shape and geometrical features [7–9]; e.g. the cell membrane potential is used in many cells to regulate their physiological functionsin particular, regulating the permeability to sodium and potassium ions in nerve and muscle tissues [10,11]. The voltage dependence of Na+ and K+ conductances requires that the channels have a sensor, such as a charge or a dipole, that responds to voltage changes [12–14]. Indeed, voltage-gated ion channels use the movement of complex voltage sensing domains to induce configuration changes elsewhere in the protein, usually generating steric occlusion of the pore domain [15,16]. These channels have been a primary source of inspiration for neuromorphic computing [17–20], as they are effectively memristors [21–23]. However, despite the great advancement of protein engineering [24–26], the precision engineering of proteins with moving parts (and related allosteric regulation) remains a formidable challenge.

Here, we focus on hydrophobically gated nanopores [7], that can modulate their transport thanks to the formation of vapor bubbles inside their lumen [27–29]. This physical gating mechanism is a rather simple and reliable way to control the current through the pore that can be modulated by an external electric field. Indeed, despite wetting of hydrophobic cavities is usually induced by the application of an external pressure [30] it is well established that an electrical field can decrease the apparent contact angle of water on top of a hydrophobic material [31,32] and that voltage can favor wetting of hydrophobic pores [33–38].

Some of the earlier work on electrowetting in hydrophobic nanopores [33,39] focused on explaining the phenomenology observed, like the fact that the permittivity of water decreased both with pore radius and applied field. They also reported an expression for the critical wetting voltage, based on energetic arguments, but found that their prediction of this voltage was 6 times higher than in their simulations. The experimental works that first showed that voltage could wet hydrophobic nanopores [36,37], also reported very interesting phenomena, like hysteresis and a critical voltage after which pores no longer dried [37]. These experiments were done using pores of nanometric radius but significantly longer (nm in simulations and μm in experiments). In both cases, the non-conductive state was explained not by a completely dry state but by local vapor/gas plugs, that would remain trapped in the pore even in the wet state. Wetting was rationalized by the creation of water bridges, or by the partial collapse of bubbles, induced by the applied voltage. For water intrusion into the pore, electrostriction, and electrostatic pressure predict wetting voltages greater than 80 V [37] and electrowetting arguments are evoked to explain a potential decrease in the contact angle of the liquid, allowing for the electrostatic pressure to complete the intrusion process. Experimental work also shows that the critical electrowetting voltage can depend on salt concentration, ionic species, and pH of the solution [38,40–42]. Simulation work [38,42] also explored charged

pores and the influence of salt species on the wetting dynamics. While these work found that specific salts could facilitate electrowetting of the pores, which is in qualitative agreement with experiments, they could not provide a definitive explanation for that result. Other works looked at simulating electrowetting in biological channels [35], doing long simulations to compute the wetting probability as well as the ion permeation-free energy at different voltages, eventually computing the current through the modeled channel. As previous works, they found that the (free) energy difference between the wet and dry state depended on the square of the applied voltage, but did not provide a comprehensive free energy profile associated with the wetting transition or how voltage influenced the wetting/drying barriers. Interestingly, they showed that proteins could generate an internal field that create asymmetries between positive and negative applied voltage. Nevertheless, no conclusive explanation or theory has been established that confidently explains the effect of voltage on the wetting properties of narrow hydrophobic pores, or gives predictions that can explain experimental or computational results, especially if one is interested in the wetting and drying rates.

Recently, hydrophobic gating and electrowetting have been combined to develop nano-fluidic memristive applications [43,44], exploiting the dependence of the wetting and drying rates on applied voltage to impart memory to the system. With the recent development of different types of iontronic memristors [17,18,45–47], together with other iontronic applications, like power generators [48], diodes [49,50], transistors [51,52], and circuits [53,54], iontronics may prove itself useful for neuromorphic applications. Real nanofluidic systems and iontronic applications have to deal with complex physical and chemical characteristics, including the presence of multiple ion species, charged pore walls, complex pore geometries, and impurities. All these effects must be taken into account to quantitatively predict the behavior of the iontronic device. Still, simplified models can be used to tackle fundamental questions, and to point to potential explanations of previously unexplained results, and to provide a solid basis for more realistic simulations aimed at testing more complex hypotheses.

In this work, we propose a general computational framework that can be used to predict how voltage influences the wetting behavior of hydrophobic nanopores – electrowetting. A simple theoretical framework informed by free-energy molecular dynamics simulations provides quantitative information on electrowetting, giving estimates for the wetting/drying kinetics and the critical voltage. This computational framework shows promise for designing new applications of hydrophobic nanopores with controlled wetting properties, including iontronic switches, nanopore sensors, and memristive devices.

Methodology

Molecular dynamics setup

Following the same protocol of our previous work [56], we built a molecular dynamics system for which we want to compute the free energy F and the diffusivity D associated with the number of water molecules N inside a hydrophobic nanopore; N represents the coarse-grained variable which defines the wetting/drying process. The system, represented in Figure 1, is made of a slab of fixed Lennard-Jones atoms in a fcc arrangement, with lattice spacing 0.35 nm, from which a cylindrical nanopore was excavated. This slab is surrounded by water

molecules (SPC/E [57]), and the water-solid non-bonded interactions are tuned [58] so that the contact angle is 104°. The nanopore has a diameter of 1.4 *nm* and a length of 2.8 *nm*. To control the pressure of the system, we used two pistons orthogonal to the pore axis [59]. The NVT ensemble was sampled using a Nosé–Hoover chains thermostat [60] at 310 K with a chain length of 3. A constant and homogeneous electric field is applied across the system $E = (0, 0, E_z)$, with z being the direction parallel to the pore axis, to mimic a difference of a constant voltage across the membrane $\Phi = E_z L_z$ [61], L_z the length of the MD box.

Free energy and diffusivity computation

We use Restrained Molecular Dynamics (RMD) [62] to compute the free energy as a function of the pore filling N. This is done by adding a harmonic restraint to the physical Hamiltonian H_{phys} of the system,

$$H_N(r, p) = H_{\text{phys}}(r, p) + \frac{k}{2} \left(N - \tilde{N}(r) \right)^2 , \qquad (1)$$

where r and p are the positions and momenta of all the atoms, respectively, k is a harmonic constant (1 kcal/mol), N is the desired number of water molecules in a box centered around the nanopore, and $\tilde{N}$ is computed by counting the number of water molecules in the region highlighted in black in Figure 1. The counting procedure has been explained in detail in a previous work [56]. The diffusivity $D(N)$, associated to the filling variable, can be computed within the same framework, being related to the integral of the autocorrelation function of $\tilde{N}$ at a given N [56].

Theory

Dependence of the free energy on the applied voltage

In this section, we explore the effect that a transmembrane voltage has on the free energy profile associated with a given collective variable θ, which in the specific case considered here is the number of water molecules inside the pore, $\theta = N$. Here, the main assumption is that the system is at equilibrium even when applying the voltage. Consider a system described by the vector x of positions and momenta of its M particles $x = (r_1, p_1, \ldots, r_M, p_M)$, with a Hamiltonian made by a 'zero voltage' part H_0 and the contribution of the external voltage Φ
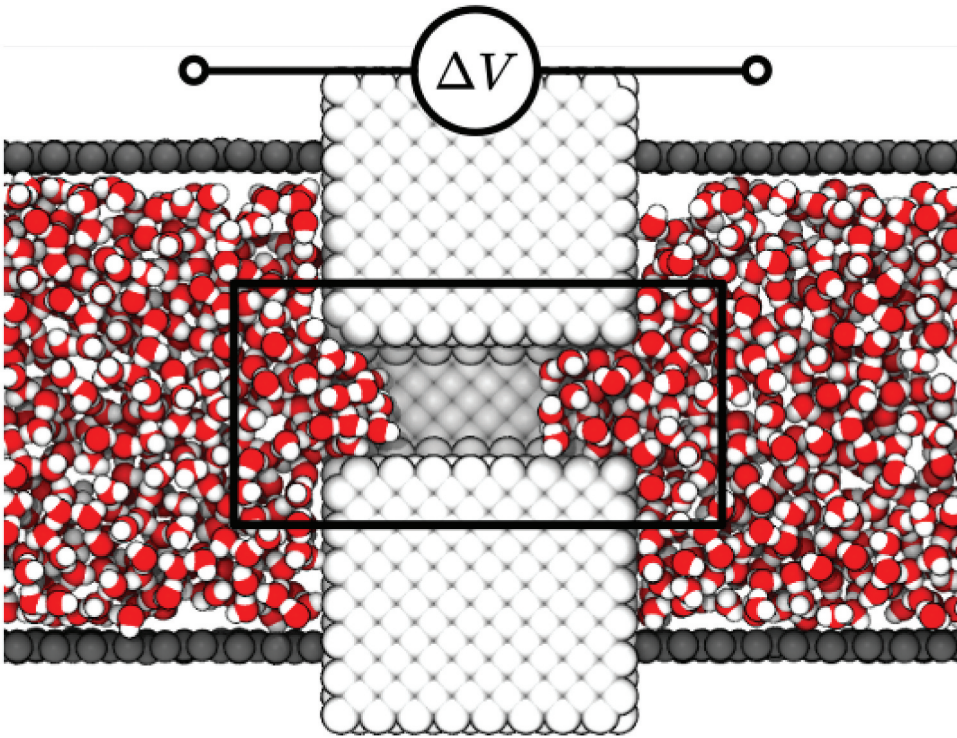
$$H(x, \Phi) = H_0(x) - Q(r)\Phi , \qquad (2)$$

with Q the displacement charge

$$Q(r) = \frac{\pi(r)}{L} , \qquad (3)$$

where

$$\pi(r) = \sum_{i=1}^{M} q_i r_i \cdot \hat{\boldsymbol{n}} \qquad (4)$$

Figure 1. System setup. Atomistic system used in this study, consisting of two reservoirs of liquid SPC/E water separated by a cylindrical nanopore drilled into a membrane formed by Lennard-Jones atoms. The lateral pistons, represented in black, composed by Lennard-Jones atoms also, are used to control the pressure by applying a force on water molecules corresponding to 1 atm. The black rectangle enclosing the pore represents the control region used to compute the water filling N and to apply the filling constrain. The voltage difference between the reservoirs is applied as an electric field that is parallel to the pore axis. The picture is realized with the VMD software [55].

is the total dipole moment of the system in the direction $\hbar$ in which the voltage is applied and L is the extension of the system in the same direction.

The probability density function of the system in the canonical ensemble is then

$$\rho(\mathbf{x}, \Phi) = \frac{1}{Z(\Phi)} e^{-\beta H(\mathbf{x}, \Phi)} \ , \tag{5}$$

with Z the partition function

$$Z(\Phi) = \int e^{-\beta H(\mathbf{x}, \Phi)} d\mathbf{x} \ . \tag{6}$$

Choosing a collective variable θ which gives a coarser description of the system, the probability density of that variable is

$$P(\theta, \Phi) = \int \delta\left(\theta - \hat{\theta}(x)\right) \rho(x, \Phi) dx = \frac{Z_\theta(\theta, \Phi)}{Z(\Phi)} \ , \tag{7}$$

where $\hat{\theta}(x)$ is the function which associates the microscopic state to a value of the collective variable, and Z_θ is the partition function restrained to a given value of the collective variable

$$Z_\theta(\theta, \Phi) = \int \delta\left(\theta - \hat{\theta}(\boldsymbol{x})\right) e^{-\beta H(\boldsymbol{x}, \Phi)} d\boldsymbol{x} \ . \tag{8}$$

The associated free energy is

$$F(\theta, \Phi) = -\beta^{-1} \log P(\theta, \Phi) \ , \tag{9}$$

and its variation with respect to voltage

$$\frac{\partial F(\theta, \Phi)}{\partial \Phi} = -\frac{1}{\beta P(\theta, \Phi)} \frac{\partial P(\theta, \Phi)}{\partial \Phi} \ . \tag{10}$$

The derivative of the coarse grained probability with respect to voltage is

$$\frac{\partial P(\theta, \Phi)}{\partial \Phi} = \int \delta\left(\theta - \hat{\theta}(x)\right) \frac{\partial \rho(x, \Phi)}{\partial \Phi} dx \ , \tag{11}$$

with

$$\frac{\partial \rho(\boldsymbol{x}, \Phi)}{\partial \Phi} = \left(\frac{\beta Q(\boldsymbol{r})}{Z(\Phi)} - \frac{dZ}{d\Phi} \frac{1}{Z(\Phi)^2}\right) e^{-\beta H(\boldsymbol{x}, \Phi)} \tag{12}$$

and

$$\frac{dZ(\Phi)}{d\Phi} = \int \beta Q(\boldsymbol{r}) e^{-\beta H(\boldsymbol{x}, \Phi)} d\boldsymbol{x} = \beta Z(\Phi) \langle Q \rangle_\Phi \ . \tag{13}$$

Hence, we obtain an expression for the derivative of the microscopic probability density with respect to voltage

$$\frac{\partial \rho(\boldsymbol{x}, \Phi)}{\partial \Phi} = \frac{\beta}{Z(\Phi)} \left(Q(\boldsymbol{r}) - \langle Q \rangle_\Phi\right) e^{-\beta H(\boldsymbol{x}, \Phi)} \ , \tag{14}$$

which can be used to compute the derivative for the coarse grained probability density

$$\frac{\partial P(\theta, \Phi)}{\partial \Phi} = \int \delta\left(\theta - \hat{\theta}(\boldsymbol{x})\right) \frac{\beta}{Z(\Phi)} \left(Q(\boldsymbol{r}) - \langle Q \rangle_\Phi\right) e^{-\beta H(\boldsymbol{x}, \Phi)} d\boldsymbol{x} \ , \tag{15}$$

simplifying

$$\frac{\partial P(\theta, \Phi)}{\partial \Phi} = \beta P(\theta, \Phi) \left(\langle Q \rangle_{\theta, \Phi} - \langle Q \rangle_\Phi\right) \ . \tag{16}$$

We finally obtain an expression for the first order derivative of the free energy with respect to voltage

$$\frac{\partial F(\theta, \Phi)}{\partial \Phi} = \langle Q \rangle_\Phi - \langle Q \rangle_{\theta, \Phi} \tag{17}$$

To obtain the second order derivative,

$$\frac{\partial F(\theta, \Phi)^2}{\partial^2 \Phi} = \frac{\partial \langle Q \rangle_\Phi}{\partial \Phi} - \frac{\partial \langle Q \rangle_{\theta,\Phi}}{\partial \Phi} \ , \tag{18}$$

we need to compute the derivative of the expected averages. Consider the generic observable A, then:

$$\frac{\partial \langle A \rangle_\Phi}{\partial \Phi} = \int A(x) \frac{\partial \rho(x, \Phi)}{\partial \Phi} \, dx \ , \tag{19}$$

we can use Equation (14)

$$\frac{\partial \langle A \rangle_\Phi}{\partial \Phi} = \int \frac{\beta A(\mathbf{x})}{Z(\Phi)} \left(Q(\mathbf{r}) - \langle Q \rangle_\Phi \right) e^{-\beta H(\mathbf{x}, \Phi)} \, d\mathbf{x} \ , \tag{20}$$

to obtain eventually

$$\frac{\partial \langle A \rangle_\Phi}{\partial \Phi} = \beta \left(\langle AQ \rangle_\Phi - \langle A \rangle_\Phi \langle Q \rangle_\Phi \right) \ . \tag{21}$$

Now we can compute the second order derivative of the free energy with respect to voltage

$$\frac{\partial F(\theta, \Phi)^2}{\partial^2 \Phi} = \beta \left(\langle Q^2 \rangle_\Phi - \langle Q \rangle_\Phi^2 - \left(\langle Q \rangle_{\theta,\Phi}^2 - \langle Q^2 \rangle_{\theta,\Phi} \right) \right) \ . \tag{22}$$

The free energy dependence on the voltage can be then approximated, up to second order, as:

$$F(\theta, \Phi) = F_0(\theta, \Phi_0) + P_1(\theta, \Phi_0)\Delta\Phi + \frac{1}{2} P_2(\theta, \Phi_0)(\Delta\Phi)^2 + const(\Phi) \ , \tag{23}$$

where $\Delta\Phi = (\Phi - \Phi_0)$, with Φ_0 being voltage around which the expansion is done; $P_1(\theta, \Phi_0) = -\langle Q \rangle_{\theta,\Phi_0}$ and $P_2(\theta) = -\beta \left(\langle Q^2 \rangle_{\theta,\Phi_0} - \langle Q \rangle_{\theta,\Phi_0}^2 \right)$; in the constant we collected all the terms that do not depend on θ, $const(\Phi) = \langle Q \rangle_{\Phi_0}\Delta\Phi + \left(\langle Q^2 \rangle_{\Phi_0} - \langle Q \rangle_{\Phi_0}^2 \right)(\Delta\Phi)^2$. While this framework is valid for a generic collective variable θ, in the following, we will focus only on the case where the collective variable is the pore filling N. During the restrained molecular dynamics simulations used to compute the free energy profiles, we computed also the values of P_1 and P_2 for different filling levels and different applied voltages.

Results

A average displacement charge and second moment of the displacement charge at 0 V

During the restrained molecular dynamics simulations used to compute the free energy, we computed the average displacement charge $\langle Q \rangle_{\theta,0}$ and its second moment, $-\left(\langle Q^2 \rangle_{\theta,0} - \langle Q \rangle_{\theta,0}^2 \right)$, which we then use to compute P_1 and P_2 in Equation (23) as a function of the water filling of the pore; data are reported in Figure 2. Because the pore shown in Figure 1 is i) symmetric, ii) uncharged, and iii) the displacement charge enters as a factor proportional to the voltage, P_1 should not

depend on the filling of the pore, as positive and negative voltages must have the same effect on wetting and drying. Molecular dynamics results indeed show that P_1 fluctuates around a constant value (Figure 2a). Differently, the amplitude of the fluctuation of P_1 sharply increases after a certain filling level, see panel b) which reports the value of the second-order coefficient P_2. This effect can be understood by considering the fact that the number of fluctuating dipoles (the water molecules) inside the pore is increasing, passing from nearly vacuum (dry) to a much more complex situation in which a larger number of molecules is present, and that can be potentially affected by the external electric field (the applied voltage drop mainly occurs inside the nanopore). Indeed, P_2 has the dimensions of a capacitance, so the second term added to the free energy could be related to the energy stored in the pore, considering it as a capacitor. In particular, the change in the stored energy depends on the filling medium: the wet pore is filled with water (relative permittivity $\varepsilon_r \gg 1$), while the dry pore is filled with vapor (i.e., for such confined geometry, vacuum with $\varepsilon_r \sim 1$). Hence, the capacitance of the dry pore has to be lower than the wet pore; we show by a dashed line what should be the energy of a capacitor with the size of the pore and a relative permittivity ε_r of c.a. 40; the latter value is lower than the bulk value due to the extreme confinement, in agreement with what has been reported for pores of sizes similar to the one studied here [33].

The fact that P_1 is constant and only P_2 depends on the filling level implies that the wetting probability of *symmetric* hydrophobic nanopores would depend only on the square of the applied voltage, and not on any linear term, because it would be the only influence on the wetting free energy, in line with what has been reported by other authors [63].
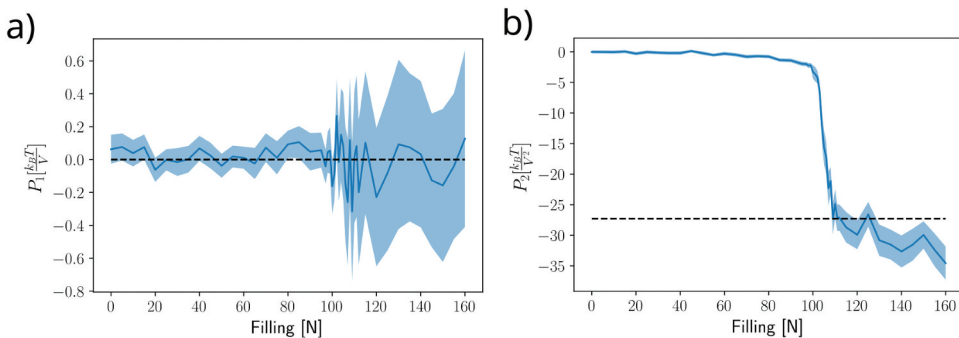

Figure 2. Values of the first order coefficient, P_1, and the second order coefficient, P_2. During the restrained molecular dynamics simulations, we computed the first and second order coefficients P_1 and P_2 of Equation (23) at different pore fillings, N. Because of the symmetry of the system, P_1 is almost constant, since opposite voltages must have the same effect. P_2 has the shape of a sigmoid function, panel b. The difference between P_2 at $N < 90$ and at $N > 90$, is related to the difference in electrostatic energy of these two states, and the dashed line represents what this difference should be if the relative permittivity of confined water, ε_r, is considered to be 40. P_1 and P_2 are shifted to zero at $N = 0$ as the free energy is always defined up to a constant. Shaded areas correspond to the 95% confidence interval computed by boostraping the averages and variances of different blocks of measurements of Q.

Effect of applied voltage on the free energy and diffusivity as a function of pore filling

We computed the free energy $F(N, \Phi)$ and the state-dependent diffusivity $D(N, \Phi)$ as a function of pore filling N at different applied voltages Φ using RMD, see Figure 3.

We remark that the free energy of a dynamical system is an equilibrium (different from steady state) quantity, hence the protocol used here is strictly valid only in the absence of electric or mass currents. For this reason, the fluid in the system of Figure 1 does not include free ions, hence our system reaches equilibrium under every applied voltage and filling constraints. Thus, the quantity we are computing corresponds to the free energy of the system, despite the applied electric field. Nevertheless, as we will explain at the end of the Conclusion section, we also simulated the nanopore system with a 0.5 M NaCl electrolyte solution, data in Fig. S2. The results show that the difference in the equilibrium-free energy profiles – with and without ions – is negligible; this fact suggests that, for such a simplified system, the contact angle is not affected at all by the presence of the ions. Also, the effect of the applied voltage on the free energy is almost the same up to 0.5 V; the interested reader will find a detailed discussion on the definition of the free energy in presence of ions moving under the electric field in the Supporting Note II.

Figure 3a shows that voltage has a non-linear effect on the free energy of the wet state. Applying $\Phi = 0.5$ V changes the free energy difference between the wet and dry state by less than $5 k_B T$ while $\Phi = 1$ V changes this difference by more than $15 k_B T$ and $\Phi = 1.5$ V by more than $30 k_B T$. The non-linear effect of voltage in wetting of hydrophobic pores has been shown previously [63] and it is in line with the prediction of our electrowetting theory, Equation (23) – as it is shown in Figures 4 and 5. We note that the position of the
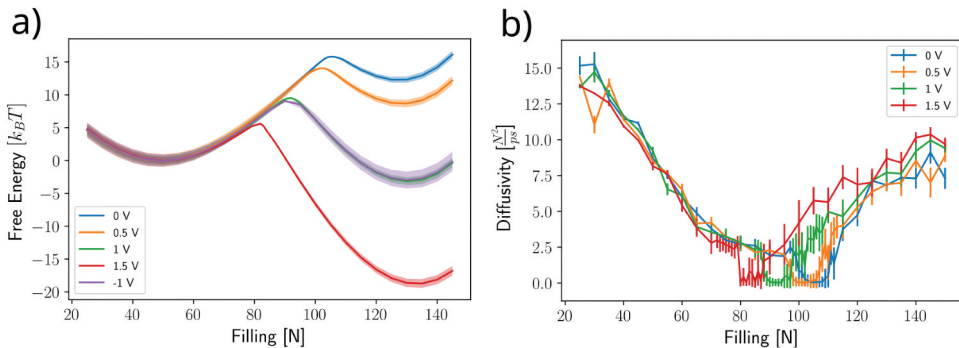

Figure 3. The effect of voltage on the free energy and the state dependent diffusivity. a) free energy as a function of the water filling for different values of applied voltage. As higher voltage is applied, the wet state becomes more and more favourable. Positive and negative applied voltages have the same effect, as can be seen from the overlap of the free energies at −1V and 1V b) diffusivity as a function of the water filling for different voltages. For most values of the pore filling, more significantly close to the two minima (dry and wet states), the voltage does not significantly change the diffusivity. Differently, it can be noted how the minimum of the diffusivity shift to lower filling level at larger voltages, following the free energy barrier maximum. The shaded area on the free energy corresponds to the error associated with the integration computed starting from the free energy barrier, by using bootstrapping to estimate the error of the derivative of the free energy. Error bars on diffusivity represent the standard error associated with two different methods.

free energy barrier changes with applied voltage, meaning that the volume (and possibly shape) of the critical nucleation bubble changes with applied voltage, requiring higher bubble volumes (corresponding to lower filling N) to make the pore dry. Panel b shows that the minimum of the diffusivity follows the maximum of the free energy barrier, shifting to lower filling levels as the voltage increases. Instead, differently from what was previously shown for the case of wetting with pressure [56], the magnitude of the diffusivity of the filling variable changes with applied voltage.

We then compared the free energy profiles computed using RMD and the ones predicted by the expansion presented in Equation (23) with respect to $\Phi_0 = 0$, see Figure 4. Panels a-d show the theoretical prediction at different voltages, $\Delta\Phi = 0.5$, 1, 1.5 and -1 V, using $F_0(N, \Phi_0 = 0)$ and the values of $P_1(N, \Phi_0 = 0)$ and $P_2(N, \Phi_0 = 0)$ shown in Figure 2. A fair agreement is found for the lowest voltage, $\Delta\Phi = 0.5$ V. However, as expected, the discrepancy becomes larger as the applied voltages increases. More specifically, the free energy differences between the wet and dry states are still well predicted at every voltage (within the estimated error) but the free energy barriers separating the wet and dry are significantly overestimated by Equation (23). Moreover, the location of the free-energy maximum does not match the correct filling level N for $\Delta\Phi > 0.5$ V. Both simulations and the predicted energy profile show that positive and negative voltages have similar free energy profiles, see Figure 4(b–d).
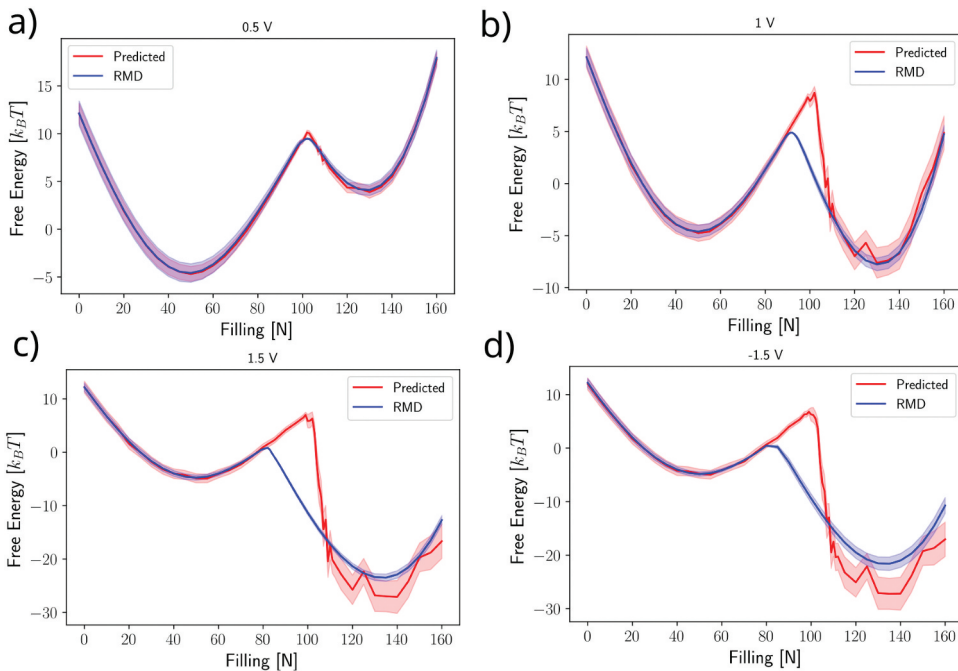
Figure 4. Comparison between free energy computed with RMD and prediction. Panels a), b), c) and d) correspond to the free energies associated with $\Phi = 0.5$, 1, 1.5 and -1 V respectively. For the lowest applied voltages, 0.5V, the predicted and computed values using RMD match, while for larger applied voltages both the barrier maximum and the free energy of the wet state are not well captured. The predicted lines (blue) use the values of P1 and P2 of Figure 2. Shaded areas correspond to the propagation of the errors 95% confidence interval computed using bootstrapping.
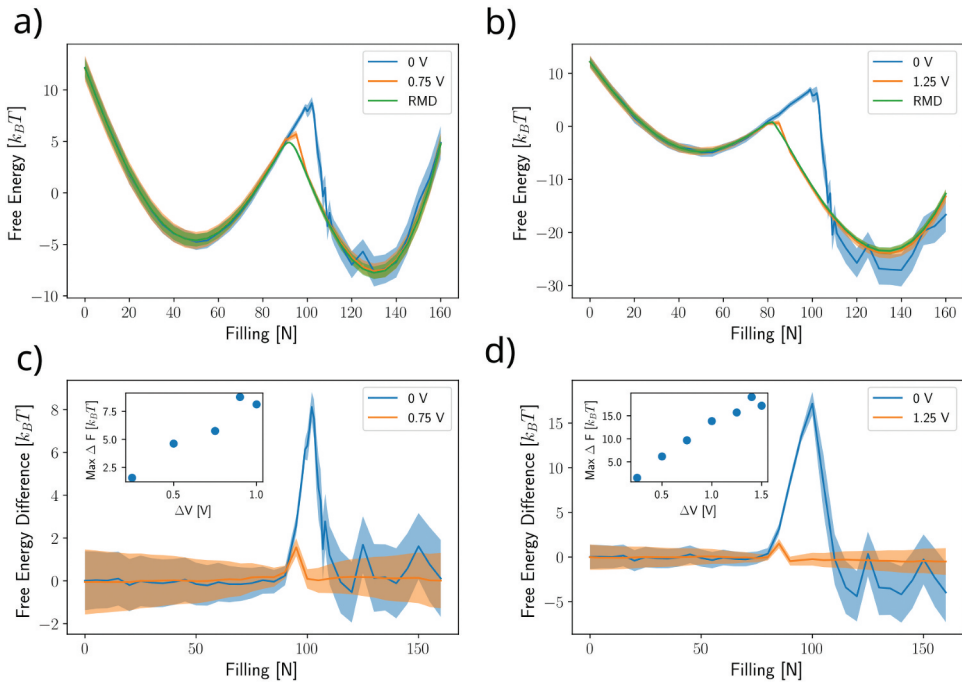
Figure 5. Predicting the free energy using a closer voltage point improves the accuracy of the model. Panel a) shows the predicting of the free energy profile at 1 V, using Equation 23, expanding around 0 V (blue) or around 0.75 V (orange). Panel b) shows the predicting of the free energy profile at 1.5 V, expanding around 0 V (blue) or expanding around 1.25 V (orange). Panel c) and shows the free energy difference between the free energy measured with RMD and the expansions at different voltages, for the case of 1 V, while panel d) corresponds to the case of 1.5 V. The insets in each panel show the maximum difference of the free energy considering expansions at different voltage differences.

The main source of error in the prediction stems from the fact that both P_1 and P_2 depend on voltage. Indeed, it is possible to improve the accuracy of the free energy prediction by computing F, P_1 and P_2 at voltages closer to the predicted one, which is equivalent to performing the Taylor expansion in Equation (23) at closer voltages, i.e. using $F_0 = F_0(N, |\Phi_0| > 0)$ and corresponding $P_1(N, |\Phi_0| > 0)$ and $P_2(N, |\Phi_0| > 0)$. As an example, in Figure 5(a,b) we compared the prediction of Equation (23) at $\Phi = 1$ V and 1.5 V, respectively, with that computed with RMD, starting from different Φ_0. In panel a) we show the predictions of $F(N, \Phi = 1V)$ by using F_0, P_1 and P_2 computed – by RMD – at $\Phi_0 = 0$ V (blue) and $\Phi_0 = 0.75$ V (orange); in panel b) the prediction for $F(N, \Phi = 1.5V)$ is done by using F_0, P_1 and P_2 measured at $\Phi_0 = 0$ V (blue) and $\Phi_0 = 1.25$ V (orange). In both cases, as expected, the theoretical expansion at smaller $\Delta\Phi = \Phi - \Phi_0$ gives much closer predictions to the free energy computed by RMD. Panels Figure 5(c,d) quantify the differences between the profiles shown in the panels a and b, respectively, for each filling level N. In both panels, it is possible to see that the largest error comes from the free energy barrier separating the wet and dry states. The insets in both panels show how the maximum difference between the free energies lowers as the theoretical expansion is performed closer to the predicted voltage, being as low as 2 k_BT for a difference $\Delta\Phi \sim 0.25$ V.

Effect of applied voltage on P_1 and P_2

As previously discussed, both P_1 and P_2 depend on the applied voltage, see Figure 6. P_1 is symmetric with respect to the applied voltage, see the green (1 V) and violet (-1 V) lines in Figure 6a. The symmetry of P_1 comes from the symmetry of the system, hence positive and negative applied voltages must have the same effect on the free energy, i.e. it must be that: $\Phi P_1(N, \Phi) = -\Phi P_1(N, -\Phi)$. Moreover, $P_1(\Phi, N)$ cannot be everywhere constant for voltages different from 0. Indeed, consider the free energy profile of the system at $\Phi = 1$ V: in that case, applying a voltage difference of $+1$ V or -1 V must give different results, because in one case you would be considering the free energy profile at 2 V, while the other you would be considering the free energy profile at 0 V.

P_1 is related to the dipole moment of the liquid inside the pore, and the interpretation of Figure 6a is that the polarization of the liquid phase is higher than that of the vapor phase, with a discontinuous jump close to the transition state. It is also possible to observe an increase of P_1 in the wet state (as N increases), with the slope depending on the applied voltage. Indeed, a larger electric field will make the water molecules more ordered, and so the total dipole moment of the liquid inside the pore will increase with the voltage; moreover, the number of ordered dipoles increases with the number of water molecules filling the pore. Even though there are no ions, differences in P_1 can be considered as differences in how much charge different states (wet vs dry) accumulate, e.g., by the rearranging dipoles of water, explaining both the increase of the magnitude of P_1 with an increase of the magnitude of the applied voltage and the fact that it must be 0 at no applied voltage, as there is no reason for charges to accumulate in a symmetrical system. On the other hand, P_2 has the same value for positive and negative voltages, see Figure 6b. As previously discussed, P_2 has the units of a capacitance and is observed to increase with the filling N in the wet state and to decrease with the applied voltage. Using the same analogy of the capacitor, this must mean that the dielectric constant of the medium goes down (as the distance and area of the plates remain the same). This result is in line with
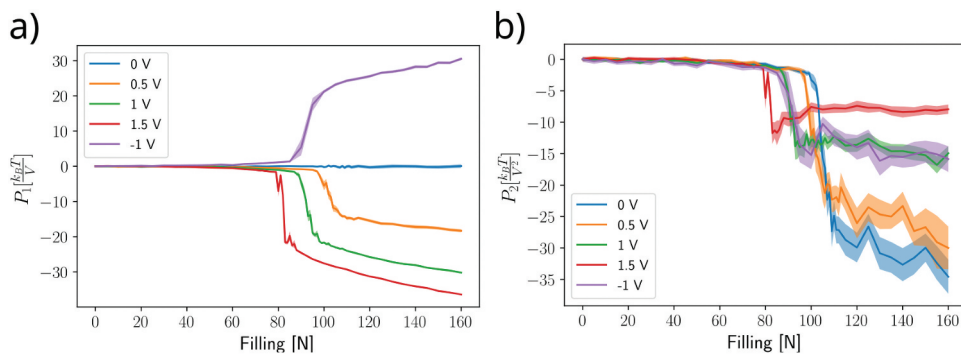
Figure 6. Dependence of P_1 and P_2 on the voltage. Panel a) shows the values of P_1 for different positive voltages and one negative voltage, highlighting its symmetric behaviour. Panel b) shows the value of P_2 for different positive voltages and one negative voltage, to highlight that positive and negative applied voltages give the same result. Both P_1 and P_2 have a step like behaviour, switching at the transition state.

previously reported data from atomistic simulations in hydrophobic nanopores, showing that the relative permittivity of water decreases with applied electric field [33]; this is linked to the disruption of the hydrogen bond network under confinement. The physical interpretations of the shapes of P_1 and P_2 are system dependent. Equation (23) can be used for different reaction coordinates, and in those cases they have to be interpreted as the added free energy that is added by voltage when the system can be characterized by that specific reaction coordinate. P_1 and P_2 may also change (in value and shape) if changes are made to the solution (e.g., by addition of ions).

As we previously demonstrated, for this particular system, our second-order expansion leads to errors lower than ca. $5 k_B T$ on the barrier only for $\Delta\Phi \leq 0.5$ V; this error is not negligible when predicting the wetting and drying rates of an hydrophobically gated switch. However, it is impractical to compute P_1 and P_2 for multiple applied voltages, because this requires computationally expensive RMD simulations. Because $P_1 = \frac{dF}{d\Phi}$, we looked for a phenomenological formula for $P_1(N, \Phi)$, which would allow us to compute directly the free energy at any Φ by integrating the expression.

To model P_1 we consider that its expression should contain some switching function that changes from a low value to a high value at a critical filling level N^*. This critical value depends on the applied voltage, and so we write it as $N^*(\Phi)$. The switching function chosen by us is a sigmoid, with expression $\frac{a(\Phi)}{1+e^{-b(N-N^*(\Phi))}}$, with $a(\Phi)$ representing a voltage-dependent amplitude. This expression does not completely capture the behavior of P_1, in particular, its increase in absolute value at higher fillings, see Figure 6a. In order to capture this trend, one can multiply the described switching function by $N^{2/3}$, a value we found to reasonably fit the simulation data. This left us to determine the expression of $a(\Phi)$, $b(\Phi)$, and $N^*(\Phi)$, which we modeled as $a = a_0 \tanh(\Phi)$, $b = 1/2$, and $N^* = N_0 - c|\Phi|$. The final expression for P_1 has the form:

$$P_1(N, \Phi) = \frac{a_0 \tanh(\Phi) N^{2/3}}{1 + e^{-\frac{(N-N_0+c|\Phi|)}{2}}}, \tag{24}$$

see the figure S1 for the fitting involved in the determination of the appropriate constants, N_0, c, a_0. The agreement between that expression and voltages not used in the fitting is shown in Figure 7.

The fitted phenomenological expression is rigorously only applicable to the specific system shown in Figure 1. We believe this expression is not a general one, especially for more complex systems, but it reasonably describes the shapes of P_1 at different voltages. Further work is needed to clarify if a more general, physically informed expression of this function exists. We believe that the arguments presented here can anyway help as guidance to fit similar phenomenological expressions in other systems, effectively speeding up the estimation of the free energy at any voltage using a minimal set of RMD simulations.

Having access to an analytical approximation of P_1 means that we can reconstruct the free energy profile at any voltage, by integrating P_1 and adding this value to the free energy at $\Phi = 0$, see Figure 8a. This approach leads to a much more accurate estimation of the free energy profile than that of Figure 4, with the maximum error at free energy barrier being less than $2 k_B T$, see Figure 8b. Despite the fact that this protocol can be used to generate the free energy profile at
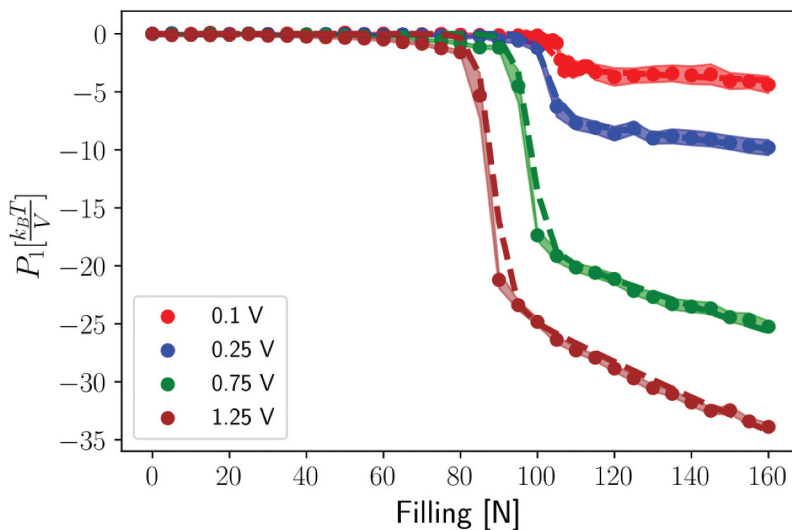
Figure 7. Accuracy of phenomenological function for P_1 and. The phenomenological function describing P_1 (dashed line) gives good agreement with the values computed with RMD (dots), for voltages not used for the fit.

arbitrary voltages, we believe that extrapolations higher than $\Delta\Phi \gg 1.5$ V will most likely give unphysical results.

Estimating the wetting and drying rates

With the idea of iontronic switches in mind, we compute the wetting and drying times at different voltages by using a rate theory expression [64] fed with the free energy profile $F(N, \Phi)$ and the state-dependent diffusivity $D(N, \Phi)$:

$$t_w(\Phi) = \int_{N_d}^{N_w} \frac{e^{\frac{F(N,\Phi)}{k_BT}}}{D(N,\Phi)} dN \int_{N_d}^{N_w} e^{\frac{-F(N,\Phi)}{k_BT}} \left(\int_{N_d}^{N} \frac{e^{\frac{F(N,\Phi)}{k_BT}}}{D(N,\Phi)} dN' \right) dN, \qquad (25)$$

with t_w being the wetting time and N_d and N_w the filling levels of the dry and wet states. To compute the drying time, one just needs to switch the integration limits. The wetting and drying rates are then computed as the inverse of the wetting and drying times, respectively. We plot the results of these calculations in Figure 9a). We observe a complete inversion of the gating behavior when voltage is applied. At low applied voltages, the system dries, i.e., switches off, much faster than it spontaneously wets, meaning that it mostly stays in the dry state. As voltage increases, the wetting rate increases, but it is still lower than $1\mu s^{-1}$ up to an applied voltage of 1 V. For higher voltages, the drying rate becomes much smaller than the wetting rate. We compare the predicted drying rates with the drying rates computed via MD simulations at two small applied voltages, finding a very good agreement. Computing these rates in such a way is highly computationally expensive and so we were not able to get an estimation of the wetting rate even at the highest voltages, because tens of simulations of multiples microseconds would be
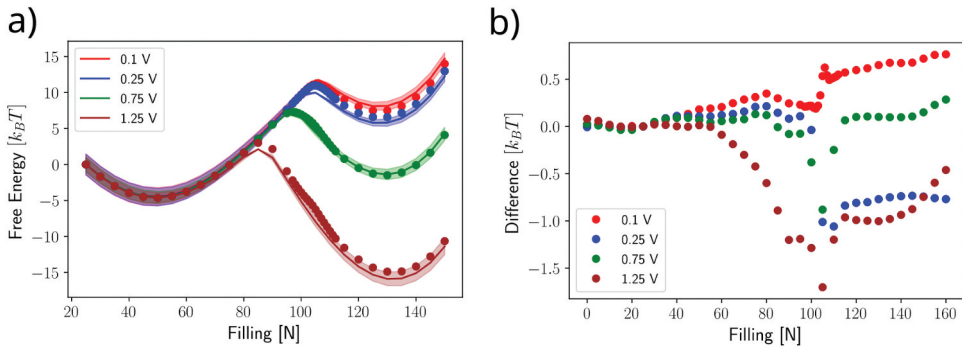
Figure 8. Free energy profile obtained from integrating P_1. The free energy profiles, panel a), computed using these expressions (full lines) are very accurate when compared with that computed using RMD (dots). The difference between the predicted and the simulated free energy, panel b), is always less than 2 k_BT, with the largest deviation located closed to the free energy barrier.

required. We also show, in Figure 9b) the probability of the system being in the wet state. This probability is given by $P_w = \frac{r_w}{r_w + r_d}$, where r_w and r_d are the wetting and drying rates. We see an abrupt transition at an applied voltage of 1 V, a critical wetting voltage comparable to what is observed in experiments. The wetting probability is important to compute because the wet state of the pore is conductive to ions, while the dry state is not, which means that voltage can be used to switch the system from a conductive to a non-conductive state, and vice-versa.
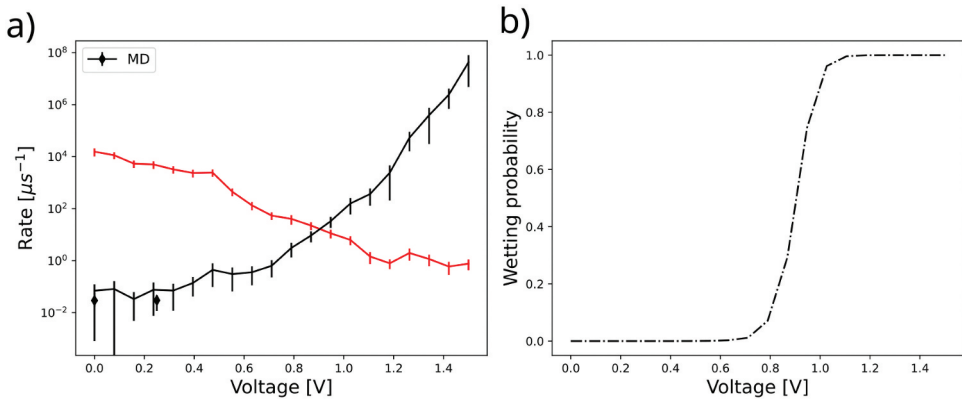
Figure 9. Wetting and drying rates at different voltages and wetting probability. In panel a) we estimate the wetting and drying rates at positive voltages, because our system is symmetric the rates at negative voltages will be the same. We also computed, using molecular dynamics, the drying rate (diamonds) for two voltages where this rate was computational accessible. Both the drying and the wetting rate change by multiple orders of magnitude. When no voltage is applied, the drying rate is 6 orders of magnitude faster than the wetting rate, while when 1.5 V is applied to the system, the wetting rate is 6 orders of magnitude faster than the drying rate. In panel b) we show the predicted wetting probability, where a sharp transition from the pores being always dry to always wet happens at around $\Phi = 1V$. The error bars on the predicted rates are the standard deviation of 100 computations of the rate, where the free energy profile and the diffusivities where sampled around their mean values and their standard deviation.

Voltage controlled switches display memristive behaviour

The fact that wetting and drying rates depend on the voltage can be exploited to develop a memristive device. We can consider what would be the behavior of an ensemble of independent hydrophobic nanopores, under different voltage protocols, by analyzing a simple master equation for the fraction of wet pores, n:

$$\frac{dn}{dt} = (1 - n)k_w - nk_d \,, \tag{26}$$

where k_w and k_d are the wetting and drying rates, respectively. Because k_w and k_d depend on voltage, we can couple this terms to arbitrary voltage protocols, simulating different experimental protocols. We chose to demonstrate, on Figure 10, what would be the response of this ensemble of pores to a saw tooth signal. Because the conductivity of the pore vanishes when there is a vapour bubble inside, and has a certain non-zero value g_0 when the pore is wet, we use $n(t)$ as a proxy for the conductivity, and do not consider any capacitive current. As expected from a memristive device, a pinched hysteresis loop is observed, whose area depends on the frequency of the applied signal (see inset). For very fast (purple), or very slow (cyan) cycling speeds, no hysteresis is observed, while for a broad range of frequencies (orange), hysteresis can be observed.

Conclusions

In this theoretical and computational work, we present a framework to predict the wetting and drying behavior of hydrophobic nanopores under an applied electric potential. Hydrophobic nanopores can be used as simple switches in nanofluidic devices because they promote the formation of a bubble that can stop the ion flux. The present framework could be used to study the behavior of other hydrophobically gated nanopores, like ion channels and biological pores.

We show that it is possible to build a theory of the effect of voltage on pore wetting, which provides the free energy at arbitrary applied voltages. By informing such theory with molecular dynamics simulations, we were able to compute the wetting free energy profiles at different voltages. This is a novel result, that goes further than the previously presented explanations that focused only on the surface energy differences and their dependence on the square of the applied voltage. Simulations at zero voltage are used to compute the coefficients P_1 and P_2 that enter into the mathematical expansion of the free energy, described by Equation 23. As expected, this expansion works best for small values of applied voltage, <0.5 V, but still predicts correctly the probability of finding the system in either the wet or dry state; the estimate of the free energy barriers, instead, becomes inaccurate as the voltage departs from zero.

Because the coefficients P_1 and P_2 depend on voltage, we computed them at different applied voltages and fit a phenomenological expression for P_1, which we could then use to accurately estimate the free energy at any intermediate value of applied voltage. The predictions are accurate even for voltages that were not used in the fitting of the phenomenological expression, with an error less than 2 k_BT at every filling point.
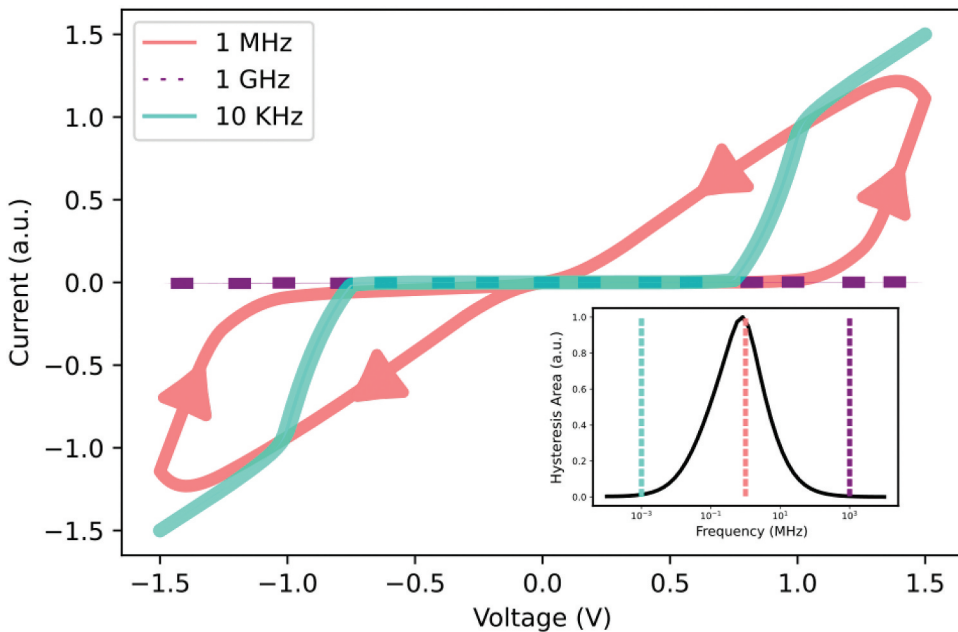
Figure 10. Memristive behaviour due to hydrophobic gating. Due to the bistability of hydrophobically gated nanopores, memristive behaviour can be observed when under voltage cycles. Depending on the cycling frequency, see inset, an ensemble of hydrophobic nanopores can behave has non-linear resistors (cyan), as resistors (purple) or as memristors (orange). The current associated with these cycles is estimated from the fraction of wet pores in the ensemble, considering that dry pores are not conductive, and that wet pores have a fixed conductivity. The fraction of wet pores was computed by integrating Equation 26, considering that a voltage signal, in the shape of a saw tooth, was applied to the system.

Our interpretation of the values of P1 and P2 and their dependence on voltage and pore geometry lead us to believe that the experimental results reporting electrowetting in long hydrophobic nanopores are due to hydrophobic gating by the formation of *local* nanobubbles [36,37,41]. On the other hand, if such long pores were completely dry, the required voltage for wetting them again would be too high. This is due to the fact that P1 and P2 would be smaller for a completely dry nanopore, while the free-energy barriers would be higher, leading to an effectively non-wettable pore. This also leads us to speculate that electrowetting in micrometer-long pores is enhanced by hydrophilic impurities inside the pores, which allow for the partial filling. We expect pores with shorter length, in the nanometer range, to always wet in the few-V range, but are not aware of any experimental work in such short solid state pores. Biological nanopores, whose dimensions are comparable to our simple system, show spontaneous wetting and drying in a way that is controlled by voltage, and it is possible to use our protocol to study such complex systems [43].

We also computed the state-dependent diffusivity for the filling variable *N* at different values of applied voltage. In this way, we were able to estimate the wetting and drying rates at different applied voltages. At low applied voltages, the pore dries in the GHz

range, while it wets only in the Hz range. We observed an inversion at high voltages, where the drying rate is 6 orders of magnitude lower than the wetting rate, while at no applied voltage the drying rate is 6 orders of magnitude larger. This means that at high voltages, the pores wet in the GHz range and dry in the Hz range.

The presence of different ion species [38], and even the ion concentration [40], has shown to be important in the wetting dynamics of pores. Ion currents can also change the temperature of fluids [65], which in turn may change their contact angle. Here, we briefly accounted for the presence of ions performing additional simulations, see Fig. S2, that show a quantitative difference from the system with no ions, mostly due to the effect of ions on P_1 and P_2 and we plan on exploring the effects of different ion species and concentrations. We plan on expanding the work on the effect of ion species and concentration. Not only that, but the present work mainly focuses on an uncharged pore, which may not be the case in all nanofluidic systems. We are also working on systems where surface charge might matter, as previously described in the literature [38,41].

The proposed framework is general and can be used to predict the voltage-controlled switching behavior of more complex hydrophobic nanopores of interest in iontronic applications. We have used this protocol to predict the memristive behavior associated with hydrophobic gating of an ensemble of hydrophobic nanopores, showing that the bistability associated with the wetting/drying transition can be exploited to impart memory to the system. We believe that hydrophobically gated memristive nanopores (HyMN's) [43] show promise as a powerful tool in the design of novel nanofluidic devices.

Disclosure statement

No potential conflict of interest was reported by the author(s).

Data availability statement

The data that support the findings of this study are openly available in Zenodo at 10.5281/zenodo.8412939

References

[1] Vincent JF, Bogatyreva OA, Bogatyrev NR, et al. Biomimetics: its practice and theory. J Royal Soc Interface. 2006;3(9):471. doi: 10.1098/rsif.2006.0127

[2] Bhushan B. Biomimetics: lessons from nature–an overview. Phys Eng Sci. 2009;367 (1893):1445. doi: 10.1098/rsta.2009.0011

[3] Arbring Sjöström T, Berggren M, Gabrielsson EO, et al. A decade of iontronic delivery devices. Adv Mater Technol. 2018;3(5):1700360. doi: 10.1002/admt.201700360

[4] Gidon A, Zolnik TA, Fidzinski P, et al. Dendritic action potentials and computation in human layer 2/3 cortical neurons. Science. 2020;367(6473):83. doi: 10.1126/science.aax6239

[5] Hille B. Progress in biophysics and molecular biology. Prog Biophys Mol Biol. 1970;21(1):1–32. doi: 10.1016/0079-6107(70)90022-2

[6] MacAulay N. Molecular mechanisms of brain water transport. Nat Rev Neurosci. 2021;22 (6):326. doi: 10.1038/s41583-021-00454-8

[7] Lynch CI, Rao S, Sansom MS. Water in Nanopores and biological channels: a molecular simulation perspective. Chem Rev. 2020;120(18):10298. doi: 10.1021/acs.chemrev.9b00830

[8] Roux B, Allen T, Bernèche S, et al. Theoretical and computational models of biological ion channels. Q Rev Biophys. 2004;37(1):15. doi: 10.1017/S0033583504003968

[9] Corry B, Chung S-H. Cellular and Molecular Life Sciences CMLS. Cell Mol Life Sci. 2006;63 (3):301. doi: 10.1007/s00018-005-5405-8

[10] Almers W. Reviews of physiology. Biochem Pharmacol. 2005;82:96–183. doi:10.1007/BFb0030498

[11] Bennett DL, Clark AJ, Huang J, et al. The role of voltage-gated sodium channels in pain signaling. Physiol Rev. 2019;99(2):1079. doi: 10.1152/physrev.00052.2017

[12] Catterall WA, Wisedchaisri G, Zheng N. The conformational cycle of a prototypical voltage-gated sodium channel. Nat Chem Biol. 2020;16(12):1314. doi: 10.1038/s41589-020-0644-4

[13] Bezanilla F. Ion channels: from conductance to structure. Neuron. 2008;60(3):456. doi: 10.1016/j.neuron.2008.10.035

[14] Hodgkin AL, Huxley AF. A quantitative description of membrane current and its application to conduction and excitation in nerve. Journal Of Physiology. 1952;117(4):500. doi: 10.1113/jphysiol.1952.sp004764

[15] Bassetto CA Jr, Costa F, Guardiani C, et al. Noncanonical electromechanical coupling paths in cardiac hERG potassium channel. Nat Commun. 2023;14(1):1110. doi: 10.1038/s41467-023-36730-7

[16] Furini S, Domene C. On conduction in a bacterial sodium channel. PLoS comput Biol. 2012;8 (4):e1002476. doi: 10.1371/journal.pcbi.1002476

[17] Xiong T, Li C, He X, et al. Neuromorphic functions with a polyelectrolyte-confined fluidic memristor. Science. 2023;379(6628):156. doi: 10.1126/science.adc9150

[18] Najem JS, Taylor GJ, Weiss RJ, et al. Memristive Ion Channel-Doped Biomembranes as synaptic mimics. ACS Nano. 2018;12(5):4702. doi: 10.1021/acsnano.8b01282

[19] Indiveri G, Linares-Barranco B, Hamilton TJ, et al. Neuromorphic Silicon Neuron Circuits. Front Neurosci. 2011;5. doi: 10.3389/fnins.2011.00073

[20] Zhu J, Zhang T, Yang Y, et al. A comprehensive review on emerging artificial neuromorphic devices. Appl Phys Rev. 2020;7(1). doi: 10.1063/1.5118217

[21] Xu Y, Ma J, Zhan X, et al. Temperature effect on memristive ion channels. Cogn Neurodyn. 2019;13(6):601. doi: 10.1007/s11571-019-09547-8

[22] Hegab AM, Salem NM, Radwan AG, et al. Neuron model with simplified memristive ionic channels. Int J Bifurcation Chaos. 2015;25(6):1530017. doi: 10.1142/S0218127415300177

[23] Chua L, Sbitnev V, Kim H. HODGKIN–HUXLEY AXON is MADE of MEMRISTORS. Int J Bifurcation Chaos. 2012;22(3):1230011. doi: 10.1142/S021812741230011X

[24] Brannigan JA, Wilkinson AJ. Protein engineering 20 years on. Nat Rev Mol Cell Biol. 2002;3 (12):964. doi: 10.1038/nrm975

[25] Huang P-S, Boyken SE, Baker D. The coming of age of de novo protein design. Nature. 2016;537(7620):320. doi: 10.1038/nature19946

[26] Zhao S, Restrepo-Pérez L, Soskine M, et al. Resolving chemical modifications to a single amino acid within a peptide using a biological nanopore. ACS Nano. 2019;13(12):13668–13676. doi: 10.1021/acsnano.9b05156

[27] Aryal P, Sansom MS, Tucker SJ. Hydrophobic gating in ion channels. J Mol Biol. 2015;427(1):121. doi: 10.1016/j.jmb.2014.07.030

[28] Yazdani M, Jia Z, Chen J. Hydrophobic dewetting in gating and regulation of transmembrane protein ion channels. J Chem Phys. 2020;153(11). doi: 10.1063/5.0017537

[29] Milenkovic S, Bodrenko IV, Lagostena L, et al. The mechanism and energetics of a ligand-controlled hydrophobic gate in a mammalian two pore channel. Phys Chem Chem Phys. 2020;22(27):15664. doi: 10.1039/D0CP00805B

[30] Giacomello A. What keeps nanopores boiling. J Chem Phys. 2023;159(11). doi: 10.1063/5.0167530

[31] Lippmann G. Ann. Chim. Phys. Ann Chim Phys. 1875;5:494.

[32] Mugele F, Baret J-C. Electrowetting: from basics to applications. J Phys. 2005;17(28):R705. doi: 10.1088/0953-8984/17/28/R01

[33] Dzubiella J, Hansen J-P. Electric-field-controlled water and ion permeation of a hydrophobic nanopore. J Chem Phys. 2005;122(23). doi: 10.1063/1.1927514

[34] Vanzo D, Bratko D, Luzar A. Dynamic control of nanopore wetting in water and saline solutions under an electric field. J Phys Chem B. 2015;119(29):8890. doi: 10.1021/jp506389p

[35] Klesse G, Tucker SJ, Sansom MSP. Electric field induced wetting of a hydrophobic gate in a model nanopore based on the 5-HT 3 receptor channel. ACS Nano. 2020;14(8):10480. doi: 10.1021/acsnano.0c04387

[36] Powell MR, Cleary L, Davenport M, et al. Electric-field-induced wetting and dewetting in single hydrophobic nanopores. Nature Nanotechnol. 2011;6(12):798. doi: 10.1038/nnano.2011.189

[37] Smirnov SN, Vlassiouk IV, Lavrik NV. Voltage-Gated Hydrophobic nanopores. ACS Nano. 2011;5(9):7453. doi: 10.1021/nn202392d

[38] Polster JW, Aydin F, de Souza JP, et al. Rectified and salt concentration dependent wetting of hydrophobic nanopores. J Am Chem Soc. 2022;144(26):11693. doi: 10.1021/jacs.2c03436

[39] Dzubiella J, Allen RJ, Hansen J-P. Electric field-controlled water permeation coupled to ion transport through a nanopore. J Chem Phys. 2004;120(11):5001. doi: 10.1063/1.1665656

[40] Innes L, Gutierrez D, Mann W, et al. Presence of electrolyte promotes wetting and hydrophobic gating in nanopores with residual surface charges. Analyst. 2015;140(14):4804–4812. doi: 10.1039/C4AN02244K

[41] Xiao K, Zhou Y, Kong X-Y, et al. Electrostatic-charge- and electric-field-induced smart gating for water transportation. ACS Nano. 2016;10(10):9703–9709. doi: 10.1021/acsnano.6b05682

[42] Polster JW, Acar ET, Aydin F, et al. Gating of hydrophobic nanopores with large anions. ACS Nano. 2020;14(4):4306–4315. doi: 10.1021/acsnano.9b09777

[43] Paulo G, Sun K, Di Muccio G, et al. Hydrophobically gated memristive nanopores for neuromorphic applications. Nat Commun. 2023;14(1):10.1038/s41467-023-44019–y. doi: 10.1038/s41467-023-44019-y

[44] Reitemeier J, Baek S, Bohn PW. Hydrophobic gating and spatial confinement in hierarchically organized block copolymer-nanopore electrode arrays for electrochemical biosensing of 4-ethyl phenol. ACS Appl Mater Inter. 2023;15(33):39707. pMID: 37579252. doi: 10.1021/acsami.3c06709

[45] Robin P, Kavokine N, Bocquet L. Modeling of emergent memory and voltage spiking in ionic transport through angstrom-scale slits. Science. 2021;373(6555):687. doi: 10.1126/science.abf7923

[46] Robin P, Emmerich T, Ismail A, et al. Long-term memory and synapse-like dynamics in two-dimensional nanofluidic channels. Science. 2023;379(6628):161. doi: 10.1126/science.adc9931

[47] Kamsma T, Boon W, Ter Rele T, et al. Iontronic neuromorphic signaling with conical microfluidic memristors. Phys Rev Lett. 2023;130(26). doi: 10.1103/physrevlett.130.268401

[48] Feng J, Graf M, Liu K, et al. Single-layer MoS2 nanopores as nanopower generators. Nature. 2016;536(7615):197. doi: 10.1038/nature18593

[49] Guo W, Tian Y, Jiang L. Asymmetric Ion Transport through Ion-channel-mimetic solid-state nanopores. Acc Chem Res. 2013;46(12):2834. doi: 10.1021/ar400024p

[50] Ma L, Li Z, Yuan Z, et al. Modulation of ionic Current rectification in ultrashort conical nanopores. Anal Chem. 2020;92(24):16188. doi: 10.1021/acs.analchem.0c03989

[51] Ren R, Zhang Y, Nadappuram BP, et al. Nanopore extended field-effect transistor for selective single-molecule biosensing. Nat Commun. 2017;8(1):10.1038/s41467-017-00549–w. doi: 10.1038/s41467-017-00549-w

[52] Park H, Baek S, Sen A, et al. Ultrasensitive and selective field-effect transistor-based biosensor created by rings of MoS2 nanopores. ACS Nano. 2021;16(2):1826. doi: 10.1021/acsnano.1c08255

[53] Maglia G, Heron AJ, Hwang WL, et al. Droplet networks with incorporated protein diodes show collective properties. Nature Nanotechnol. 2009;4(7):437. doi: 10.1038/nnano.2009.121

[54] Bayoumi M, Bayley H, Maglia G, et al. Scientific reports **7**. 2017. doi: 10.1038/srep45167

[55] Humphrey W, Dalke A, Schulten K. VMD: Visual molecular dynamics. Journal Of Molecular Graphics. 1996;14(1):33–38. doi: 10.1016/0263-7855(96)00018-5

[56] Paulo G, Gubbiotti A, Giacomello A. An atomistically informed multiscale approach to the intrusion and extrusion of water in hydrophobic nanopores. J Chem Phys. 2023;158(20). doi: 10.1063/5.0147647

[57] Berendsen H, Grigera J, Straatsma T. The missing term in effective pair potentials. J Phys Chem. 1987;91(24):6269. doi: 10.1021/j100308a038

[58] Camisasca G, Tinti A, Giacomello A. Gas-induced drying of nanopores. J Phys Chem Lett. 2020;11(21):9171. doi: 10.1021/acs.jpclett.0c02600

[59] Marchio S, Meloni S, Giacomello A, et al. Pressure control in interfacial systems: Atomistic simulations of vapor nucleation. J Chem Phys. 2018;148(6):064706. doi: 10.1063/1.5011106

[60] Martyna GJ, Klein ML, Tuckerman M. Nosé–Hoover chains: the canonical ensemble via continuous dynamics. J Chem Phys. 1992;97(4):2635. doi: 10.1063/1.463940

[61] Gumbart J, Khalili-Araghi F, Sotomayor M, et al. Constant electric field simulations of the membrane potential illustrated with simple systems. Biochim Biophys Acta - Biomembr. 2012;1818(2):294. doi: 10.1016/j.bbamem.2011.09.030

[62] Maragliano L, Vanden-Eijnden E. A temperature accelerated method for sampling free energy and determining reaction pathways in rare events simulations. Chem Phys Lett. 2006;426(1–3):168. doi: 10.1016/j.cplett.2006.05.062

[63] Trick JL, Song C, Wallace EJ, et al. Voltage gating of a biomimetic nanopore: electrowetting of a hydrophobic barrier. ACS Nano. 2017;11(2):1840. doi: 10.1021/acsnano.6b07865

[64] Hänggi P, Talkner P, Borkovec M. Reaction-rate theory: fifty years after Kramers. Rev Mod Phys. 1990;62(2):251. doi: 10.1103/RevModPhys.62.251

[65] Tsutsui M, Arima A, Yokota K, et al. Ionic heat dissipation in solid-state pores. Sci Adv. 2022;8 (6):10.1126/sci- adv.abl7002. doi: 10.1126/sciadv.abl7002